**Global Journal of Chemistry, Biology and Physics**
Volume.9, Number 5; September-October, 2024;
ISSN: 2836-8207 |
Impact Factor: 6.62
https://zapjournals.com/Journals/index.php/gjcbp
Published By: Zendo Academic Publishing

# A STUDY OF THE OPTICAL PROPERTIES AND URBACH TAIL OF SPRAY-DEPOSITED TIO₂ THIN FILMS AT DIFFERENT VOLUMES FOR OPTOELECTRONIC APPLICATIONS.

**[1]Y.Tanko, [2]M.Y Onimisi, [2]H Ali, [1]B.Y. Zakariya, [3]H.A. Lawal and [4]Kurawa S.M[4]**
*Corresponding E-mail: yunanatanko01@gmail.com*

**Article Info**

**Keywords:** Dielectric, refractive index, absorption coefficient, urbach, band tail.

DOI
10.5281/zenodo.13842590

## Abstract

In this study, titanium dioxioxide ($TiO_2$) was produced stoichiometrically using an easier and cost-effective spray pyrolysis technique (SPT). The effect of microstructure and phase formation of $TiO_2$ thin films at different volumes is investigated by XRD analysis. XRD investigation depicts that the $TiO_2$ contents correspond to the anatase phase. XRD study also shows that the pure $TiO_2$ at different content samples are nanostructured. A phase transition, anatase phase to mixed phase, was confirmed from the XRD when the $TiO_2$ content increased (0.5, 1.0 1.5 and 2.0) $cm^3$. A thorough investigation of microstructural and dispersion parameters was carried out. The results revealed that when the content concentration was increased from 0.5 to 2.0 at $cm^3$, the crystallite size ranged from $D_S = 0.162$ to 0.186 nm, $\delta s = 38.104$ to 28.90 nm, while the strain was found to decrease from $\varepsilon = 2.933$ to 0.7486, $\times 10^{-3}$. From the UV vis spectra, it is evident that the maximum absorbance values for different volumes of $TiO_2$ (0.5, 1.0, 1.5, and 2.0) occur in the ultraviolet region at a wavelength of 300nm with a corresponding intensity of (-0.2 to 1.31) a.u., with absorption edges at the visible region of 400nm, shifted towards a longer wavelengths, resulting in the reduction of bandgap energy from 3.36eV to 3.27eV with corresponding decrease in the urbach energy displayed from 45.99eV to 12.30eV. The equivalent band tail contribution arising from the weak absorption tails with a maximum value obtained was 2.220 eV. The dispersion and oscillatory energy decrease abruptly with increasing $TiO_2$ content, exhibiting the same phase of transition momentum. Other optical parameters like dielectric constants, refractive index, extension coefficient (k), absorption coefficient, and thermal conductivity are estimated.

---

[1]Department of Physics, Kaduna State college of Education Gidan Waya, Kaduna, Nigeria.
[2] Department of Physics, Nigerian Defense Academic, Kaduna, Nigeria.
[3] Department of Physics, Air Force Institute of Technology, Kaduna, Nigeria
[4] Department of Physics, Sa adatu Rimi university of education, Kano, Nigeria.

## Introduction

Titanium dioxide $TiO_2$ thin films are the most widely used coating materials because of their desirable properties, such as good adhesion, high stability against mechanical abrasion, chemical attachment, and high temperature. In general, Materials made of transparent conducting oxide (TCO) are very interesting because of their unique optical, chemical, physical, and optoelectronic characteristics. Because of its high refractive index, chemical stability, resistance to photo corrosion, low cost, nontoxicity, and strong photocatalytic activity, $TiO_2$ is the most promising TCO material among the others in a number of study areas [1].

The majority of research has examined the relationship between $TiO_2$ particle size and photocatalytic activity, and it has been found that $TiO_2$ films' photocatalytic activity increases as particle size decreases [2]. Nonetheless, anatase, rutile, and brookite are the three primary crystalline forms of titania that occur naturally. The most efficient photocatalyst is a combination of anatase and a smaller amount of rutile [3]. Rutile alone is not a strong photocatalyst. $TiO_2$ with anatase phase as a TCO has numerous benefits because of its inexpensive cost, stability in a hydrogen plasma atmosphere, and relatively low effective mass, which are used to construct solar cells [4]. The microstructural and optical properties of $TiO_2$ have evolved significantly in order to harness the complete solar spectrum for numerous uses and tackle our environmental problems [5].

A wide range of applications for photocatalytic activity have been examined and described in the literature in recent years. Photoreactors of the flow type for self-cleaning and purifying water Highway tunnel lamps and glass covers coated with $TiO_2$ are two examples of these. [6][7]. Nanocrystalline $TiO_2$ films can be made in a number of ways: The Sol-Gel method, enhanced chemical vapor deposition (PECVD) [7], metal organic decomposition (MOD) [9], physical vapor deposition [8], and so on. Among them, the spray-pyrolysis process has many advantages over traditional synthesis techniques, such as better crystalline phase, uniformity, purity, and chemical control [10]. The differences in characteristics between rutile, anatase, and amorphous thin films have sparked a lot of interest in the investigation of their growth processes. Oxygen defects, impurities, and crystalline size all have an important effect on the optical characteristics of $TiO_2$ films. The deposition process and the thermal treatments applied afterward play a crucial role in causing thin films to exhibit the desired characteristics. $TiO_2$ is technologically significant in thin film form for applications such as light emitting devices and flat panel displays; thus, luminescence emission from $TiO_2$ nanopowders and nanowires [12,13]. Some authors have reported on the optical and micro characteristics of rare-earth $TiO_2$ thin films [14, 15].They have come to the conclusion that one of the main difficulties in designing an appropriate coating process for use in particular applications is structural control. In this paper, we present a spray-pyrolysis approach that uses spin coating technology to manufacture nanocrystalline $TiO_2$ thin films. This method is widely accepted as the most straightforward, cost-effective, and high-quality method for synthesizing thin-film materials. In addition, we conducted elemental analysis to ascertain the impact of varying $TiO_2$ volumes on surface form, optical characteristics, and structural characteristics.

The current investigation focuses on the optical and microstructural characteristics of titanium dioxide thin films produced at different content levels. The different microstructural properties were determined while considering line broadening using the Scherrer and Stokes-Wilson formula in combination with the Wemple and DiDomenico (W–D) model. To the best of our knowledge, there are no thorough studies available on the measurement of dispersion energy, band tailing, and optical characteristics in connection to different $TiO_2$ impurity levels. Consequently, the average oscillator strength, dielectric constants, refractive index, Urbach energy, and Urbach tail have become major areas of study for the present generation of scholars. Based on these observations, it appears that the goods in their current state could be a promising alternative for optoelectronic applications.

## 2.0 Experimental details

### 2.1 Materials

Zinc powder and HCl (2mol) were used to etch fluorine-doped tin oxide (FTO) coated glass substrates (2.5x 2.5mm) in order to provide 0.224cm$^2$ of active electrode area. The substrates underwent soap cleaning, methanol and distilled water rinsing, and compressed air drying. Then, using a titanium isopropoxide solution diluted in ethyl acetone, a $TiO_2$ blocking layer was applied to the substrates by spray pyrolysis at $350^{°C}$. Titanium isopropoxide (0.0075 m) and acetone (0.15 mol) were used to prepare the samples. The titanium isopropoxide was mixed with 0.15 mol (0.06 g) of the solvent ethyl acetone before being added to the isopropyl alcohol, which served as the solvent. To reduce the impact of humidity, titanium isopropoxide was injected into the mixture. The mixed precursor was sprayed on the glass substrate, which had been heated to $350^{oC}$, using an atomizing voltage machine with 6 kV output. The substrate-to-nozzle distance was 8mm. To produce diverse substrate thicknesses, four different precursor volumes (0.5, 1.0, 1.5, and 2.0 ml) were sprayed on various substrates, each volume flow's duration (4.11, 4.50, 5.43, and 9.20) min/sec was also recorded. Therefore, v/t (m/s) was used to calculate the flow rate. The films were maintained at $350^{°C}$ for 5 min following each stage of spraying. Here are the schematics; it's clearly showed in figure 1.0(b) that the flow rate is found to be directly proportional to the volume content.

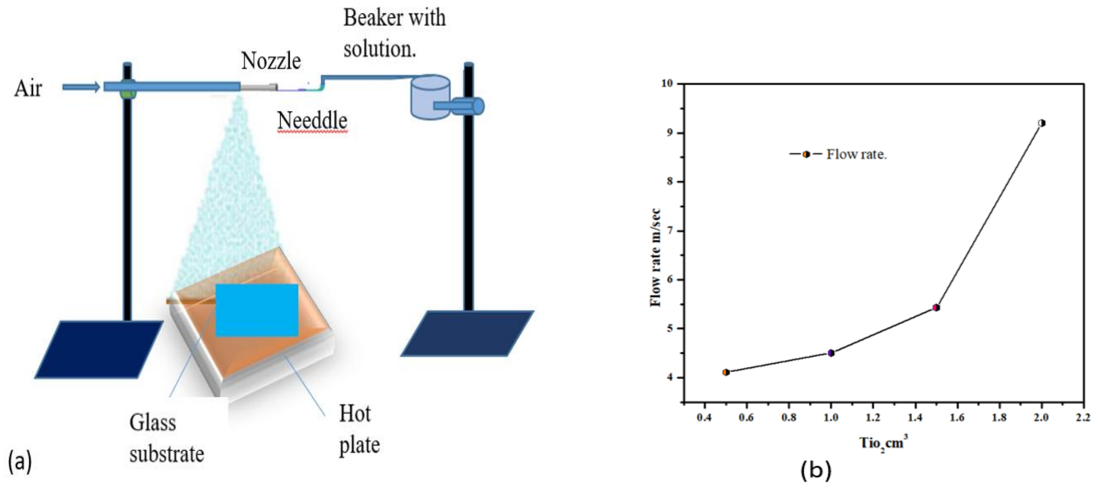

Fig 1.0(a) Experimental setup of the spray pyrolysis technique and fig 1.0(b) showing the flow rate.

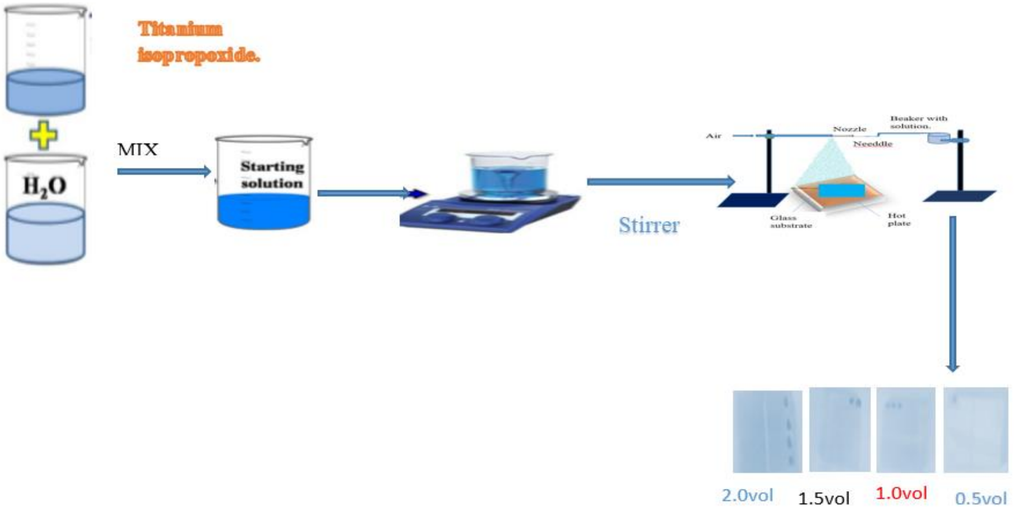

|Deposited $TiO_2$ at different content

Figure (2.0): Plausible diagram of $TiO_2$ thin films at different volumes.

Hydrolysis of metal alkoxides results in the formation of metal oxide ($TiO_2$) particles. The following describes the general reaction that could occur on a heated substrate between titanium isopropoxide (precursor) and water (reactant), forming a $TiO_2$ thin film.

$$Ti\ (OC_4H_9)4 + 4H_2O \rightarrow Ti(OH)_4 + 4C_4H_9OH \qquad (1)$$

$TiO_2$ is then formed by condensation of the hydrolyzed species.

$$Ti(OH)_4 \rightarrow TiO_2 + 2H_2O \uparrow \qquad (2)$$

## 2.3 Characterization techniques

We describe the $TiO_2$ thin-films optical and structural characteristics. Phase identification and crystallinity were examined using an XRD diffractometer (3040XPertPRO, Philips). The absorbance spectra of the items were detected using a UV-Visible-NIR spectrophotometer to further ascertain their optical characteristics.

## 3.0 Results and discussion

### 3.1 Microstructural investigations.

Figure 3.0 displays the XRD patterns of all thin film samples of $TiO_2$ at different volumes of 0.5, 1.0, 1.5, and 2.0. The obtained XRD peaks at 0.5 volume confirmed the anatase phase of the tetragonal crystal arrangement having space group I41/and (JCPDS 21-1272) [16], and the highly tensed peak indicates the good crystallinity of $TiO_2$ nanoparticles. The product is observed to display a mixed phase of $TiO_2$ and transition from the anatase to the rutile phase upon the addition of additional $TiO_2$ content levels (0.5, 1.0, 1.5, and 2.0) volume. The $TiO_2$ nanoparticles exhibit a preferred orientation and constructive development along the (101) plane. As shown in Fig. 3.0, the prominent peak shifts toward higher 2θ positions, demonstrating that the increased impurity content of $TiO_2$ caused the anatase to convert to the rutile phase [17].

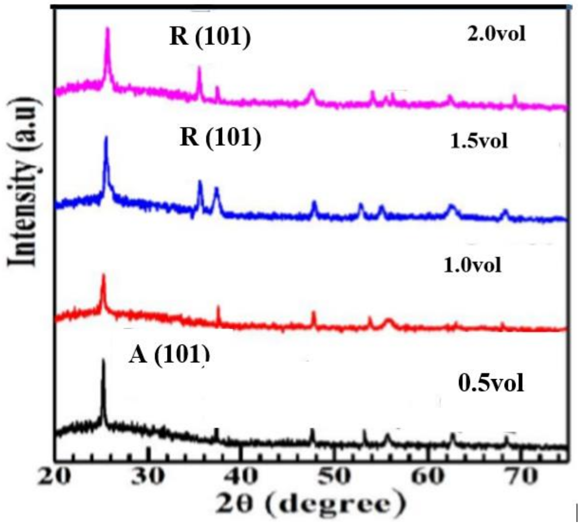

**Figure (3.0): XRD patterns of $TiO_2$ thin films at different volumes.**

### 3.1.1 Calculation of D using Scherrer formula

Examining the crystallite size (D) and lattice strain (ε) is essential for understanding its nanocrystalline characteristics. Several methods for estimating these attributes have been developed. FWHM and the peak of the planes from the XRD data in the Debey-Scherrer equation [18] were the initial methods used to estimate the D values for different $TiO_2$.

$$D_{S=}\,{}^{K\lambda}/_{\beta COS\theta} \qquad (3)$$

Where $D_s$ = crystallite size, $\lambda$ = wavelength of x-ray radiation ($\lambda$=1.54056 Å for Cu-K$\alpha$), $\beta$ = half-width full maximum, $\theta$ = Bragg's angle in degrees, and K = 0.09. Table (3) displays the estimated values of Ds. Figure (4.0) shows the evolution of the dislocation density and crystallite size Ds. It is evident that the inverse relationship is maintained. The size of the crystallites increases with increasing $TiO_2$ concentration, but the dislocation density shows the reverse pattern. In general, the higher the dislocation density, the smaller the crystals.

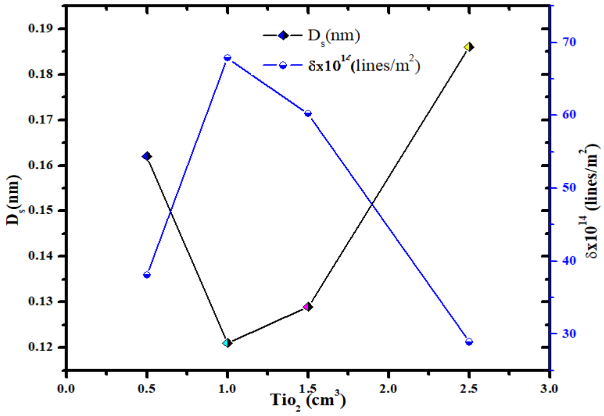

**Figure** (4.0): **Variation of crystalline size and dislocation density as a function of different content of $TiO_2$**

### 3.1.2 Estimation of the Effective Dispersion Energy Profile For $TiO_2$ Nanoparticles

Analyzing the dispersion properties of $TiO_2$ thin films is essential because it provides valuable insights for designing practical optical communication and spectral dispersion devices. Determining if $TiO_2$ thin films are a viable option for real-world applications requires an understanding of the material's dispersive behavior. The W–D model, developed by Wemple and DiDomenico, has been utilized. The refractive index is shown in accordance with this concept using the relation shown below [19]. The dispersion energy parameter, $E_d$, represents the average strength of the interband optical transitions, and the single oscillator energy, $E_0$, indicates the average bandgap energy. The energy dispersion parameter $E_d$ is related to ionicity, anion valency, efficient number of diffusion electrons, and harmonization of positive ions adjacent to one another [20][21].Considering equation (4), a diagram of $(n^2 -1)^{-1}$vs $(h\nu)^2$ has been depicted in Fig. 17. By estimating the y-intercept and slope from the $(n^2 -1)^{-1}$ vs $(h\nu)^2$ plot, the values of $E_d$ and $E_0$ are calculated.

$$n^2 - 1 = \frac{E_0 E_d}{E_0^2 - (h\nu)^2} \qquad (4)$$

The 0.5 sample, which starts the thin film's structural alterations, has the greatest value of $E_d$ [22].It imply that the co-ordination number of atoms reduces as the value of $E_d$ falls (for 1.0, 1.5, and 2.0). Similarly, as $TiO_2$ content rises, the value of $E_0$ falls; this could be because of a drop in band gap energy and an increase in scattering centeredness [8].

### 3.1.3 Dispersion of optical constant.

Figure 5.0 demonstrates the optical absorbance of $T_iO_2$ at different volumes, in which 0.5 volumes were mostly preparable in solar cell fabrication because of its higher absorption capacity.

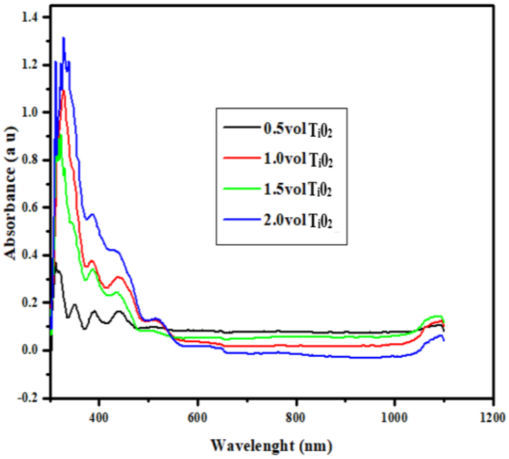

**Figure 5.0 Optical absorbance of $TiO_2$ at different volumes.**

Figure 5.0 displays the optical absorbance spectrum of $TiO_2$ thin films, which was captured in the spectrum of wavelengths between 300nm and 1200nm. As a result, it is evident that the maximum absorbance values for different volumes of $TiO_2$ (0.5, 1.0, 1.5, and 2.0) occur in the ultraviolet region at a wavelength of 300nm with a corresponding intensity of (-0.2 to 1.31) a.u., and the absorption edges at the visible region of 400nm are also displayed. With reference to the aforementioned Figure 7.0, it is evident that a substrate with 2.0vol and 1.0vol of $TiO_2$ has lower absorbance values of 1.3au and 1.1au, respectively, in the ultraviolet region 350nm, whereas greater absorbance occurs at 1.5 and 0.5 vol of $TiO_2$ in the same wavelength spectrum. Generally, as $TiO_2$ vol increases, the absorbance value decreases. This outcome was in line with previous research [26]. It claims that the absorbance value of thin films is decreased by $TiO_2$ vol. This is because photons are absorbed by electrons and transferred from the valence to the conduction band at the fundamental transition area [27]. In addition, it was noted that the optical absorption steadily reduced from the UV to the near IR area. It was found that the excitation of electrons from titanium's valence band to its conduction band causes light to be absorbed, leading to a considerable decrease in the wavelength value [28].

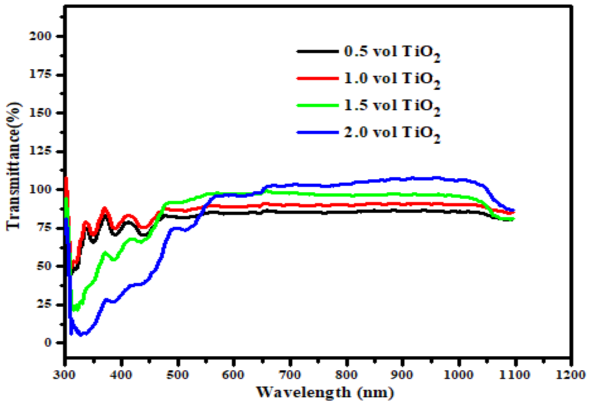

**Figure 6.0: Optical Transmittance of $TiO_2$ at different volumes.**

The transmittance spectra of $TiO_2$ film at various volumes (0.5, 1.0, 1.5, and 2.0) and wavelengths spanning 300–1200 nm are shown in Figure 6.0. According to the preceding figure, transmittance increases significantly when $TiO_2$ volume on the substrate increases between 400 and 500 nm, after which it maintains a steady transmission within the same wavelength range.

This indicates that the transmittance value in the thin films increases with increasing $TiO_2$ volume. Nonetheless, the transmittance remained constant in the 380–800 nm (ultraviolet–visible) wavelength range because photons with energy below the band gap could not excite electrons; therefore, they could only be transmitted [29]. A film's crystal quality was also correlated with its transmittance value. Besides being influenced by the quality of the crystal film, it was clearly shown that the transmittance value was also influenced by the amount of $TiO_2$ spraying on the substrates, which is in accordance with a research conducted by [30].

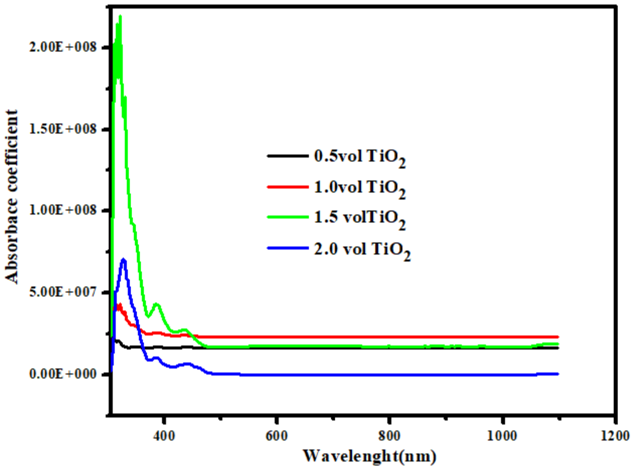

**Figure 7.0 Variation of the Absorption Coefficient with Wavelength at Different Volumes of $TiO_2$**

As the $TiO_2$ volume increases, Figure 7.0 demonstrates that absorption also increases; the maximum absorption capacity is found at 1.5 vol. $TiO_2$ at varied contents absorbed at the same wavelength spectrum but with different absorption edge values in the ultraviolet region of the electromagnetic spectrum. In addition, it was shown that $TiO_2$ had the highest absorption capacity values at 1.5 vol.

This could be due to an increase in the size of the active particles, which would then increase the charge transfer from the titanium cations' valence band to their conduction band and result in a higher absorption coefficient [31].

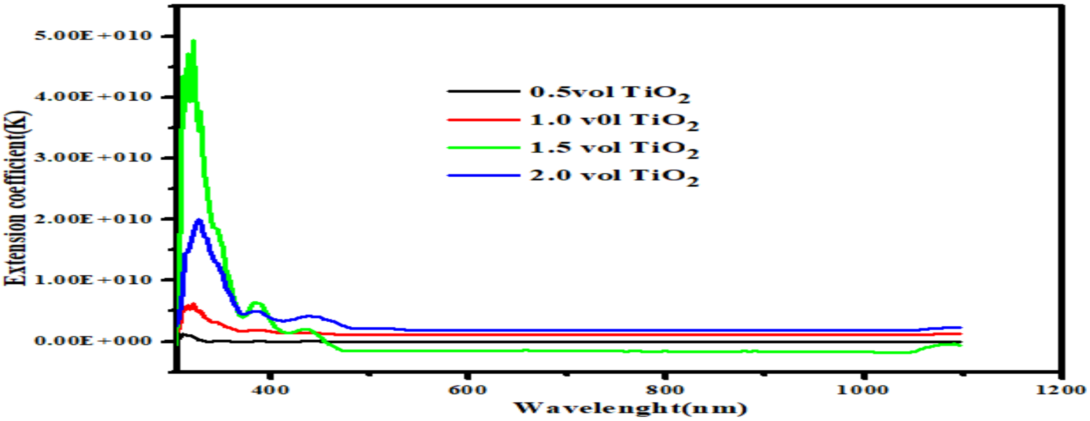

**Figure 8.0, Variation of Extension Coefficient (k) of $TiO_2$ With Wavelength at different volumes.**

The extension coefficient (k), which was determined from the absorbance data for $TiO_2$ at different volumes using equation (10) is displayed in Figure 8.0. The percentage of energy lost to scattering and absorption per unit thickness in a given medium is known as the extension coefficient (k). It is apparent that the extension coefficient is more prominent at 1.5 and 0.5 volumes of $TiO_2$. Nonetheless, the higher values of the extension coefficient (k) at long wavelengths imply that the addition of $TiO_2$ results in greater photon scattering, which is consistent with the findings of [32].

$$\bar{n} = n + ik \qquad (10)$$

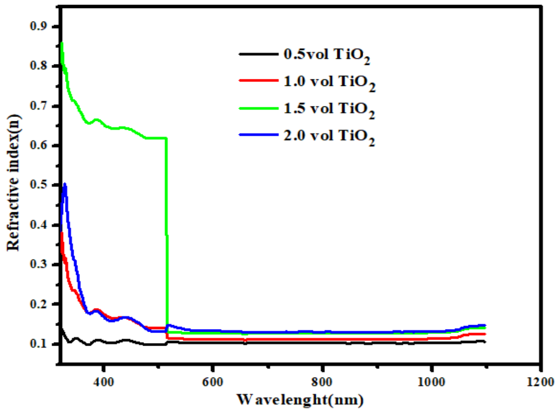

**Figure 9.0 Variation of Refractive index(n) With Photon Energy at Different $TiO_2$ Volumes**.

Figure 9.0 displays the refractive index dispersion (n) for different $TiO_2$ volumes in the wavelength range 300–1200 nm. Equation (11), derived from the absorbance data, was used to compute the dispersion. The refractive index (n), which in $TiO_2$ can reach values of 0.85, clearly increases with volume in $TiO_2$ thin films, as shown in Figure 9.0. At 0.5 volumes, the refractive index of $TiO_2$ is lowest, corresponding to a dispersive index of 0.15. At 1.5 volume of $TiO_2$, on the other hand, the thin film dispersion increases. As the wavelength increases, the refractive index decreases significantly and becomes saturated beyond the wavelength of 1000 nm, as seen in figure 9.0 above. The high-wavelength area of the refractive index (n) indicates the bulk properties of the material. The sharp rise in the refractive index (n) for $TiO_2$ volume could be attributed to the percolation threshold phenomenon [33].

$$n = \frac{1+\sqrt{R}}{1-\sqrt{R}} \qquad (11)$$

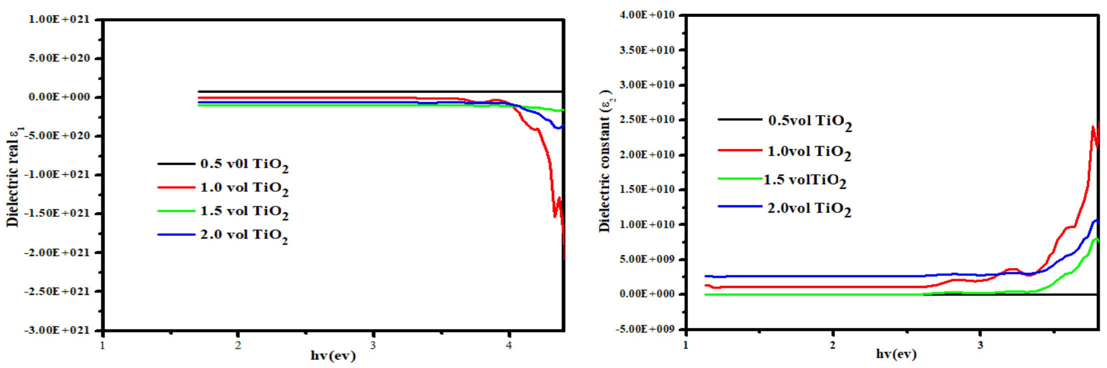

(a) (b)

**Figure(10.0):** The real and imaginary ($\varepsilon_2$) dielectric constant variations with photon energy

The real and imaginary ($\varepsilon_2$) dielectric constant variations with photon energy at different $TiO_2$ volumes are shown in Figures 10.0(a) and (b). Figure 10.0(a) shows that the dielectric constant is higher at low photon regions and approaches a near constant value before rapidly decreasing with additional photon energy [25][34]. The conventional dielectric response, in accordance with Koop's theory, demonstrates a high dielectric constant value in the low-photon region, indicating a reduction in the dielectric constant with increasing photon energy and an almost constant (relaxation behavior) at the high-photon region [26][35]. On the other hand, as the photon energy increases in figure 12.1(b), the imaginary dielectric constant abruptly increases and remains constant at low photon energies. Ionic, electronic, orientation, and space charge polarizations are the four types of total polarization that are present in nanocrystals [25][36]. The dipolar polarization and space charge polarization are highly dependent on the concentration and temperature, which also affect the high dielectric constant value. Grain size increases with increasing $TiO_2$ content, but as a result, the density of grain boundaries decreases, and at high photon energy, the relaxation of the grain boundary appears to be suppressed or merges with a grain, as shown in figure 12.0 (a) [36]. Both the relaxation behavior in the low photons and the contributions from the grain boundary are subdued. Due to $TiO_2$ content increment, the interfacial polarization at lower photons also increases, which is the region of more charge accumulation and charge transfer on the grain boundaries.

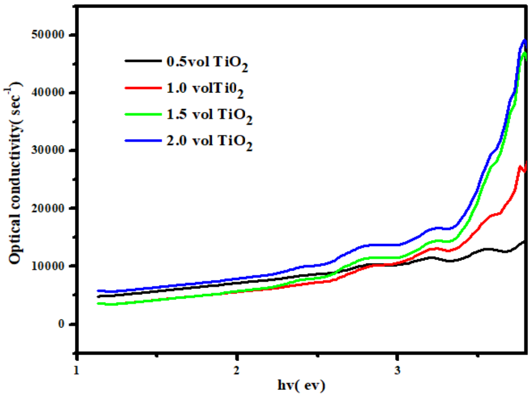

**Figure 11.0 Variation of Optical Conductivity (sec$^{-1}$) with Photon energy of $TiO_2$ at different volumes**

Equation (12) was used to compute the optical conductivity of $TiO_2$ films. Figure 11.0 shows the fluctuation of optical conductivity (opt) with photon energy for $TiO_2$. It is evident that thin films made of $TiO_2$ have good optical conductivity with an increase in photon energy. Because the optical conductivity (opt) was calculated using the absorption coefficient, an increase in optical conductivity at high photon energies might be caused by the high absorbance of $TiO_2$ thin films as well as by the excited electrons that result from the photon energy [37]. The optical conductivity of all the $TiO_2$ samples sharply increased, as seen in figure13.0, indicating a high excitation of electrons. It was found that the conductivity is at its lowest level, ranging from 4000 to 6000s$^{-1}$. This low level of electrical conductivity is a result of the charge carriers' reduced mobility due to ionic size, which changes the electronic band structure. As a result, as more energy is applied, the optical conductivity of the formed $TiO_2$ crystal increases [15].

$$\sigma_{opt} = \alpha n c / 4\pi \qquad (12)$$

### 4.4.0 Band gap Energy and Urbach Energy in $TiO_2$ Films.

The absorption coefficient in the Tauc technique is typically used to calculate the band gap. In this procedure, the band gap was typically calculated using the absorption coefficient. Equation (13), which uses the Tauc equation to measure the band gap energy [38].

$$\alpha = \frac{A(hv - E_g)^{1/2}}{hv} \qquad (13)$$

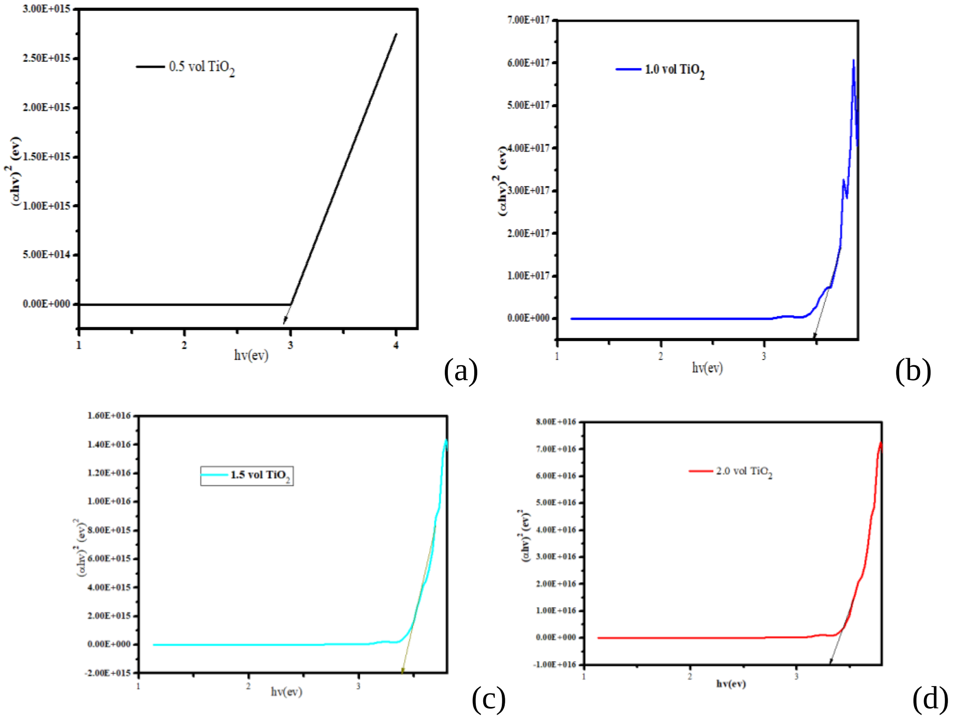

(a) (b)

(c) (d)

**Figure 12.0: Plot of $(\alpha hv)^2(eV)^2$ versus hv(ev) at different $TiO_2$ contents**

Plots of the photon energy (h)(eV) versus the volume of $TiO_2$ (0.5, 1.0, 1.5, and 2.0) samples are shown in Figure 12.0 (a, b, c, and d). Extrapolating a curve's linear segment until it intersects with an abscissa yields the band gap energy. For various samples of $TiO_2$, the predicted direct band gap energy values are displayed in table 4.0 below, correspondingly. With 0.5 vol of $TiO_2$, the band gap energy is predicted to be 2.93eV in figure 14.0(a). The band gap energy for 1.0 vol of $TiO_2$, depicted in Figure 12.0 (b), has an estimated value of 3.39 eV. This discovery demonstrates that the band gap energy decreases with increasing $TiO_2$ volume, with the exception of 0.5 volume, as shown in figures 12.0(c) and (d) with 1.5 and 2.0 volumes of $TiO_2$ and corresponding band gap energies of 3.29 and 3.27 eV, respectively. It has been shown that with additional volume, the grain size grows and the film crystallinity improves, which in turn decreases the band gap energy. Increase in particle size leads to molecular structural disorder defects and residual strain. A deposition error could also be responsible for the significantly reduced band gap energy at 0.5 vol of $TiO_2$. This aligns with the research of [39]. Table 4.0 lists the conclusions reached for band gap energy using the Tauc technique.

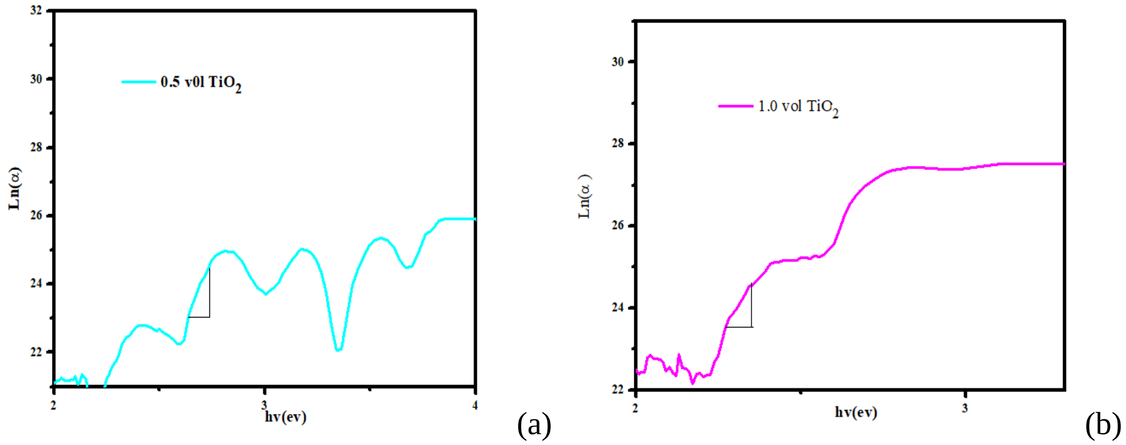

(a) (b)

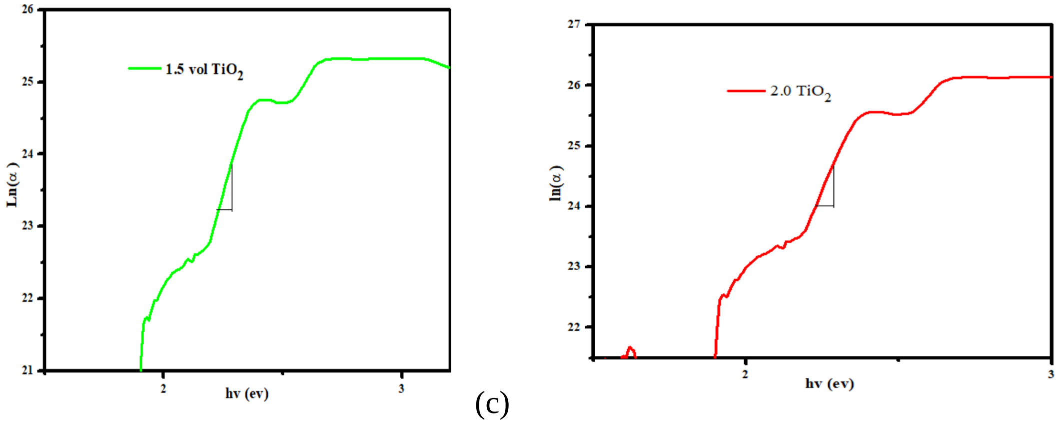

(c) (d)

**Figure 13.0: Plot of Ln(α) versus hv(ev) at different TiO$_2$ contents.**

Ln(α) versus hv(eV) variation at various TiO$_2$ volume concentrations for the Urbach energy measurement is shown in Figure 13.0 (a, b, c, and d). Plotting ln(α) vs. hv and fitting a straight line to the linear part of the curves allowed us to determine the urbach energy. Equation (14) was used to calculate $E_u$, which is the value produced by taking the reciprocal of the slope of this linear region. With 0.5 vol of TiO$_2$, the urbach energy is shown in Figure 13.0 (a) and was calculated to be 45.99 eV. The calculated urbarch value for 1.0 vol of TiO$_2$ was found to be 16.68 eV, as shown in Figure 13(b). The calculated urbarch energy values were discovered to be 5.827eV and 12.30eV, respectively, in figures 13 (c) and (d) for 1.5 and 2.0 volumes of TiO$_2$. The results of the analysis above showed that the urbach energy values fall as the crystal and molecule sizes of the thin films increase, with the exception of the value at 0.5 vol, which indicates a high degree of disorderliness at the lower volume of TiO$_2$. This could be due to the regular multiple exiton transition that occurs in thin films. Therefore, as the volume increases, the stability of the thin films increases, which in turn causes the disorderliness of the particles to decrease, which accounts for the drop in Urbach energy at 1.0, 1.5, and 2.0 volumes [39] The table 4.0 below shows the estimated values for the band gap energy and urbach energy of TiO$_2$ at various volumes.

$$\alpha(hv) = \alpha_o e^{(hv/E_u)} \qquad (14)$$

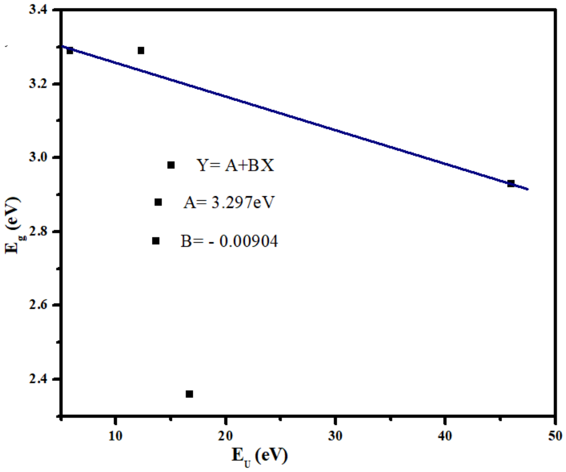

**Figure 14.0 Relationship between the Bandgap Energy and the width of the Urbach tail for TiO$_2$ thin films deposited at different volumes.**

It is observed that the band gap decreases as the value of $E_u$ increases, the small value of the urbach energy may be due to the less disorderliness of the thin film, and the decrease in the band gap as the urbach energy increases may be due to an increase in the dispersion of grain size, which causes the band gap to decrease. A linear fit was constructed because there was a small difference between the real world in terms of the Urbach energy, band gap energy, and band tailing. The band gap energy at $E_g = 0$ or the band gap in the absence of tailings is represented by the constant A resulting from the fit. The obtained value for the substrate at various TiO2 contents is 3.297 eV, and these values are consistent with the band gap energy at the early stage. In line with the well-known behavior of semiconductors, it is clearly shown that the band gap value in the absence of tailings decreases with an increase in the substrate content. This finding validates the rationale provided above for why the band gap energy decreases as the substrate content of $TiO_2$ increases. That is, films with a larger content of $TiO_2$ have higher order and a lower density of localized states.

**Table 4.0: Optical band gap and urbach energy values of $TiO_2$**

| S/N | Ti0$_2$ (cm$^3$) | $E_g$ (eV) | $E_U$(eV) | $E_t$=$E_g$ -$E_u$ (eV) | $E_g$ =$E_u$+$E_t$(eV) |
|---|---|---|---|---|---|
| | | | | | |
| **1.0** | 0.5 | 2.93 | 45.99 | -43.06 | 2.93 |
| **2.0** | 1.0 | 3.36 | 16.68 | -14.32 | 2.36 |
| **3.0** | 1.5 | 3.29 | 5.825 | -2.535 | 3.24 |
| **4.0** | 2.0 | 3.27 | 12.30 | -9.01 | 3.27 |

## 3.4 Conclusion

In conclusion, a general synthesis and characterization of pure $TiO_2$ thin films at different contents has been presented, and a cost-effective spray pyrolysis route has been employed to meticulously synthesize the samples. XRD analysis shows that the pure $TiO_2$ samples at different contents are nanostructured. A phase transition, anatase phase to mixed phase, was confirmed from the XRD when the $TiO_2$ content increased (0.5, 1.0 1.5 and 2.0) cm$^3$. A thorough investigation of microstructural and dispersion parameters like crystallite size, strain, dislocation density oscillatory, and dispersion energy, was performed using Sherers, Stokes–Wilson formula, and DiDomenico (W– D) model. The investigated results revealed that when the content concentration was increased from 0.5 to 2.0 at cm$^3$, the crystallite size was in the range from $D_s = 0.162$ to 0.186 nm, $\delta s = 38.104$ to 28.90 nm, while the strain was found to decrease from $\varepsilon = 2.933$ to 0.7486, ×10-3. According to the UVvisible spectra, the maximum absorbance values for the various volumes of TiO2 (0.5, 1.0, 1.5, and 2.0) are clearly visible in the ultraviolet region at a wavelength of 300 nm, with a corresponding intensity of (-0.2 to 1.31 a.u. The absorption edges at the visible region of 400 nm are shifted toward longer wavelengths, which causes the bandgap energy to decrease from 3.36 eV to 3.27 eV and the urbach energy to drop from 45.99 eV to 12.30 eV. Furthermore, the bandgap energy of $TiO_2$ determined by UV-vis diffuse reflectance spectra, which has a value of 2.92 eV, is strongly correlated with the corresponding band tail contribution resulting from the weak absorption tails, with a maximum value obtained to be 2.220 eV. The dispersion and oscillatory energy show the same phase of transition momentum as they quickly decrease as the $TiO_2$ content increases. Estimates are made for additional optical properties such as thermal conductivity, refractive index, extension coefficient (k), dielectric constants, and absorption coefficient. Thin films of $TiO_2$ may be considered as an effective and promising candidate in manufacturing and designing electronic devices.

**Acknowledgement:**

We would like to express our gratitude to the Nigerian Defense Academy Kaduna (NDA) Department of Physics for their kind assistance, the Kaduna State College of Education for their financial support, and the Nigerian Research Institute Shesko Abuja for providing the equipment needed to conduct this special research project.

**Declaration:**

We affirm that there is no financial interest in the subject matter or materials covered in this paper and that this work has not yet been submitted to any journal. We further state that we have no affiliations or involvements with any party.

**References.**

Yang Juan, M.E., Sen, and J.M.F. Ferreira (2001), Hydrothd, Synthesis of nanosized Titania powders: Influence of tetra alkyl ammonium hydroxides on particle characteristics, J. Am. Ceram. Soc. 84(8), 1696-1706.

Ruan, S.F. Wu, T. Zhang, W. Gao, B. Xu, and M. Zhao, (2004), Surface state of $TiO_2$ nanoparticles and photocatalytic degradation of methyl orange in aqueous $TiO_2$ dispersions, Mater.chem.phys, 69, 7-9.

Touam T, Atoui M, Hadjoub I, Chelouche A, Boudine B, Fischer A, Boudrioua A and Doghmane A (2014) Effects of dip-coating speed and annealing temperature on structural and morphological and optical properties of sol-gel nano-structured $TiO_2$ thin films EPJ Appl Phys 67 30302–6

Houng B, Liu C. C. and Hung M.T. (2013) Structural, electrical and optical properties of molybdenum-doped $TiO_2$ thin films Ceramics International 39 3669–76.

Magdalane C. M, Kanimozhi K, Arularasu M V, Ramalingam G and Kaviyarasu K (2019) Self-cleaning mechanism of synthesized $SnO_2/TiO_2$ nanostructures for photocatalytic activity application for wastewater treatment Surfaces and Interfaces 17 100346

Liu. S, and X. Chen, (2008). A visible light response $TiO_2$ photocatalyst realized by cationic S-doping and its Application for phenol degradation, J.Hazard.mater, 152(1), 48- 55.

Chen, C.W. Zhu, T. Yu, and X. Chen and X. Yao, (2003) Preparation of metal organic Decomposition Derived strontium zirconate dielectric thin films, Appl. Surf. Sci. 2111, 244-249.

Taurino,A. M. Epifani, T. Toccoli, S. Iannotta and P. Siciliano,(2003) Innovative aspects in thin film technologies for nanostructure materials in gas sensor devices Solid Films. 436, 52–63.

Rothschild, A. F. Edelman, Y. Komem and F. sandy, (2000) Sensing behavior of $TiO_2$ thin films Exposed to air at low temperatures, Sensor. Actuat B-Chem. 67, 282-289.

Kim D H, Hong H S, Kim S J, Song J S, Lee K S (2004) Photocatalytic behaviors and structural characterization of nanocrystalline Fe-doped $TiO_2$ synthesized by mechanical alloying Journal of Alloys and Compounds 375 259–64

Fidelus J.D.M. Barezak, k. micchalak Z. Fekner, A. Duzynska, A. JusZa, Rapira, midowicz C.J. monty, A. Suchocki, Journal of Nanoscience, Nanotechnol.12 (2012) 3760 -3765.

chinnamuthu, A. Modal, N.K. Singh, J.C. Dhar, S.K. Das k.k chaltopadhyay, Journal of Nanosci. Nanotechnol 12(2012) 6445 -6453.

Merino, R.P. A.C. Gallardo, M.G.Rocha, I. H. Calderon, V. Castano, R. Rodriguez, thin solid films 40, (2001) 118-123

Jia C.E. Xie, A. Peng R. Jiang F.H. Lin, T. Xu, thin solid films 496(2006) 555 -559.

Weng, W., Ma, M., Du, P., Zhao G, Shen G, Wang, J. and Han, G. (2005) Super hydrophilic Fe doped TiO2 thin films prepared by spray pyrolysis deposition Surface & Coatings Technology 198 340–4.

Jereil, S. D. and Vijayalakshmi, K. (2015) Effect of Fe doping on the properties of $TiO_2$ thin films for ethanol sensing application Nano Vision 5 69–76

Kumar P M R, Kartha C S, Vijayakumar K P, Abe T, Kashiwaba Y, Singh F and Avasthi D K (2005) On the properties of indium doped ZnO Semiconductor Sci Technol 20 120.

Datta J, Layek A, Das M, Dey A, Middya S, Jana R and Ray P .P (2017) Growth of hierarchical strontium-incorporated cadmium sulfide for possible application in optical and electronic devices Journal of Materials Science: Materials and Electronics 28 2049–61

Usha K. S, Sivakumar R. and Sanjeeviraja C. (2013) Optical constants and dispersion energy parameters of NiO thin films prepared by radio frequency magnetron sputtering technique. J Appl Phys 114 123501

Wemple S. H and DiDomenico M. (1971) Behavior of the electronic dielectric constant in covalent and ionic materials. Physical Review B 3: 1338–1351.

Sen S K, Paul T C, Manir M S, Dutta S, Hossain M N and Podder J (2019) Effect of Fedoping and post annealing temperature on the structural and optical properties of - MoO3 nanosheets Journal of Materials Science: Materials in Electronics 30 14355– 14367

Dhanapandian S, Arunachalam A. and Manoharan C. (2016) highly oriented and physical properties of sprayed anatase Sn-doped $TiO_2$ thin films with enhanced antibacterial activity Applied Nanoscience 6 387–97

Arunachalam A, Dhanapandian S, Manoharan C. and Sridhar R. (2015) Characterization of sprayed $TiO_2$ on ITO substrates for solar cell applications Spectrochimica Acta - Part A: Molecular and Biomolecular Spectroscopy 2015;149:904–12.

Reneldi, V., V., Rajendan, (2012). Synthesis characterization of Nano-$Tio_2$ via different method, Apply. Sci. Research 4, 2, 1183–1190.

Kumar, M.H, Dharani, S., Leong, W.L., Ricardo, (2014) Lead-free halide perovskite solar cells with high photocurrents realized through vacancy modulation. Adv Mater. 26, 7122–7127.